

# On the complementarity of ordinal patterns-based entropy and time asymmetry metrics

Cite as: Chaos **33**, 033138 (2023); <https://doi.org/10.1063/5.0136471>

Submitted: 26 November 2022 • Accepted: 01 March 2023 • Published Online: 22 March 2023

 Johann H. Martínez,  José J. Ramasco and  Massimiliano Zanin

## COLLECTIONS

Paper published as part of the special topic on [Ordinal Methods: Concepts, Applications, New Developments and Challenges](#)



View Online



Export Citation



CrossMark

## ARTICLES YOU MAY BE INTERESTED IN

### [A new coding system to test independence of time series](#)

Chaos: An Interdisciplinary Journal of Nonlinear Science **33**, 013122 (2023); <https://doi.org/10.1063/5.0132097>

### [Ordinal methods for a characterization of evolving functional brain networks](#)

Chaos: An Interdisciplinary Journal of Nonlinear Science **33**, 022101 (2023); <https://doi.org/10.1063/5.0136181>

### [Selecting embedding delays: An overview of embedding techniques and a new method using persistent homology](#)

Chaos: An Interdisciplinary Journal of Nonlinear Science **33**, 032101 (2023); <https://doi.org/10.1063/5.0137223>



**Chaos**  
Special Topic: Nonlinear Model  
Reduction From Equations and Data  
**Submit Today!**

# On the complementarity of ordinal patterns-based entropy and time asymmetry metrics

Cite as: Chaos 33, 033138 (2023); doi: 10.1063/5.0136471  
Submitted: 26 November 2022 · Accepted: 1 March 2023 ·  
Published Online: 22 March 2023



View Online



Export Citation



CrossMark

Johann H. Martínez,<sup>1,2,a)</sup>  José J. Ramasco,<sup>2</sup>  and Massimiliano Zanin<sup>2</sup> 

## AFFILIATIONS

<sup>1</sup>Instituto de Matemática Interdisciplinar, Departamento de Análisis Matemático y Matemáticas Aplicadas, and GISC, Universidad Complutense, Plaza de las ciencias, 3, 28040 Madrid, Spain

<sup>2</sup>Instituto de Física Interdisciplinar y Sistemas Complejos IFISC (CSIC-UIB), Campus UIB, 07122 Palma de Mallorca, Spain

**Note:** This paper is part of the Focus Issue on Ordinal Methods: Concepts, Applications, New Developments and Challenges.

**a)** Author to whom correspondence should be addressed: johemart@gmail.com

## ABSTRACT

Entropy and time asymmetry are two intertwined aspects of a system's dynamics, with the production of entropy marking a clear direction in the temporal dimension. In the last few years, metrics to quantify both properties in time series have been designed around the same concept, i.e., the use of ordinal patterns. In spite of this, the relationship between these two families of metrics is yet not well understood. In this contribution, we study this problem by constructing an entropy–time asymmetry plane and evaluating it on a large set of synthetic and real-world time series. We show how the two metrics can at times behave independently, the main reason being the presence of patterns with turning points; due to this, they yield complementary information about the underlying systems, and they have different discriminating performance.

Published under an exclusive license by AIP Publishing. <https://doi.org/10.1063/5.0136471>

**Entropy and temporal asymmetry are two cardinal facets of any dynamical system. Statistical physics has long been studying their mutual relationship from a theoretical point of view; yet, the numerical quantification of these two concepts in real-world systems has advanced along parallel but separate paths, with the potential interplay between them remaining largely unclear. In this contribution, we tackle this issue by reconstructing an entropy–time asymmetry plane, juxtaposing two metrics calculated on time series symbolized through the concept of ordinal patterns. We show how this plane is an adequate phase space to better comprehend and track situations in which entropy and time asymmetry behave in independent or complementary ways; and we evaluate it through both synthetic and real-world time series.**

## I. INTRODUCTION

Among the numerous techniques developed in the last few decades for the analysis of time series, the concept of ordinal (or

permutation) patterns has been attracting increasing attention, starting from some initial works focusing on the analysis of ordinal data.<sup>1</sup> A milestone was achieved 20 years ago by Christoph Bandt and Bernd Pompe when in a seminal paper<sup>2</sup> they showed that the complexity of a time series could be estimated through the statistics of suitable defined ordinal patterns. In short, the time series under analysis is first divided into sub-windows; elements thereof are then reordered in an ascending order; and, last, a symbol is associated with each sub-window, representing the permutation performed in the previous step—a more complete description of the methodology is provided in Sec. II A. The method, thus, allows one to synthesize a time series into a sequence of discrete symbols, representing the relative amplitude relationships between neighboring values. Besides its conceptual simplicity, the Bandt and Pompe approach presents several additional advantages, such as the low sensitivity to observational noise, and the weak requirement of stationarity in the time series under analysis. Additionally, it allows unveiling properties of the underlying dynamical system, e.g., its stochastic vs chaotic nature,<sup>3</sup> in a simple way. Not surprisingly, this resulted in an ever increasing number of research works using this methodology, both

theoretical and applied—the interested reader can refer to multiple reviews available in the literature.<sup>4–8</sup>

One of the simplest ways of analyzing the obtained sequence of symbols is to calculate its entropy, e.g., through the classical Shannon entropy. As its classical counterpart, the permutation entropy then describes how predictable (from an ordinal point of view) the dynamics under analysis is. Statistical physics also provides a complementary concept known as time irreversibility, i.e., the idea that the dynamics of a system may be recognizable (and, hence, significantly different) from its time reversed version. If entropy quantifies the uncertainty about the future evolution of a system, its irreversibility measures how much entropy it produces as time passes<sup>9</sup> and quantifies the degree of nonlinear dependencies (memory) in it.<sup>10</sup> In the last few years, among the many alternative approaches to quantify it,<sup>11</sup> several research groups have independently proposed ways to adapt the irreversibility concept to the ordinal framework, with the common idea that it must appear as an imbalance between the frequency of ordinal patterns that are pairwise time symmetrical.<sup>12–16</sup> As the stationarity of the time series is not always taken into account, the term time asymmetry is here used, to differentiate it from a more strict definition of irreversibility.

One question that has still to be tackled in the literature is whether these two derived metrics based on ordinal patterns, i.e., entropy and time asymmetry, are overlapping, or, on the contrary, yield complementary views on the underlying dynamical system. While these two concepts are clearly differentiated in statistical physics, in spite of the common origin, they are here calculated as similar aggregations of ordinal pattern frequencies. In other words, while the permutation entropy quantifies the variability in ordinal pattern frequencies, the time asymmetry focuses on the variability between pairs of time-symmetric patterns. The question then boils down to understanding whether the different aggregations of ordinal patterns hide relevant information.

By building on the well-known concept of the entropy-complexity plane,<sup>17</sup> we here propose the reconstruction of an entropy-time asymmetry (HTa) plane and study the similarities and differences between these two metrics using a set of synthetic and real-world time series. Results suggest that both metrics, while related, are not the same. Specifically, some dynamical systems can be discriminated according to one of them, but not necessarily according to the other. Additionally, we show that, while observational noise always increases entropy, it can increase the time asymmetry when the underlying dynamics is characterized by a large share of ordinal patterns with turning points. We finally evaluate the HTa plane using real data representing biological, economic, and technological systems.

## II. METHODS

The HTa plane represents, in its vertical axis, the level of randomness of the output of the dynamical system under study and, in its horizontal one, its variability when moves forward and backward over time. In other words, the plane assumes that a dynamical system can be characterized in terms of how much its entropy changes as a function of its irreversibility transition when both aspects are captured by means of order patterns. In what follows, we first introduce how ordinal patterns are calculated; for then defining the

**TABLE I.** Graphical representation of the  $D! = 6$  available symbols  $\pi$  of length  $D = 3$ . Each symbol is defined by the different ranking of the elements of the vector under analysis.

$\pi_0$	$\pi_1$	$\pi_2$	$\pi_3$	$\pi_4$	$\pi_5$

corresponding entropy and time asymmetry metrics; and finally reviewing the synthetic time series that will be used in the evaluation.

### A. Ordinal patterns

Ordinal patterns can be considered an alphabet to describe a dynamical system's output  $x_t$ , which has proven to be especially effective in the case of time series with a finite and limited number of observations (samples)  $M = \|\{x_t\}\|$ . The idea behind its construction is to define a  $D$ -length vector,  $D$  being usually called the embedding dimension. The vector is composed of values of  $x$  starting at a given time point  $t$ ; and values can be consecutive or not depending on the value of the lag (or delay) parameter  $\tau$ . The vector is then associated with a symbol  $\pi$  by comparing the relative inner amplitudes and representing the permutation required to sort values in increasing order. In other words,  $\pi$  contains no information about the absolute amplitudes of values, but instead, it represents the relative amplitude of the elements composing the  $D$ -vector  $\{x_t, x_{t+\tau}, \dots, x_{t+D\tau}\}$  by ranking them such that  $(x_{t+\tau\pi_0} \leq x_{t+\tau\pi_1} \leq \dots \leq x_{t+\tau\pi_{D-1}})$ . As a result, each permutation is a letter of the system's alphabet (see Table I for a graphical representation for  $D = 3$ ); and a complete time series can then be synthesized into the discrete probability distribution  $p(\pi)$  of the symbols' abundance.

Note that the extraction of ordinal patterns depends on two parameters, the embedding dimension  $D$  and the embedding lag  $\tau$ . Regarding the former, the maximum  $D$  that can be used is closely related to the length  $M$  of the time series, as enough instances of each ordinal pattern have to be observed to obtain reliable statistics; hence, a rule of thumb suggests that  $M \gg (D + 1)$ !<sup>18</sup> Second, while most research works focused on  $\tau = 1$ , it has been shown that different embedding lags can help unveil the system's characteristic time scale.<sup>19–21</sup> For the sake of simplicity and without loss of generality, we will here consider  $\tau = 1$ .

### B. Entropy and time asymmetry

The empirical distribution  $p(\pi)$  of  $x_t$  is used to calculate the Shannon entropy  $S = -\sum_{\pi} p(\pi) * \log(p(\pi))$ . Without loss of generality, we here compare the uncertainty as measured by  $S$ , with the maximum uncertainty  $S_{\max}$  that would be obtained if all  $\pi$  were equally probable; i.e.,  $p(\pi_i) = 1/D!$ . This maximum is trivially given by  $S_{\max} = \log(D!)$ . The so-called permutation entropy is then obtained following this normalization as

$$H[p] = S/S_{\max}, \quad (1)$$

which by construction is normalized in  $0 \leq H[p] \leq 1$ .

Parallel to this, the concept of the system time asymmetry is based on the level of imbalance between the information content when the system evolves forward  $p(\pi)$  vs backward  $p'(\pi)$  in time. Note that the latter is calculated by simply time-reversing the original time series such that  $x'_t = x_{M-t+1}$  with  $t \in [1, M]$  and then evaluating the ordinal patterns  $\pi$  over  $x'$ . Leveraging on this idea, the time asymmetry can be estimated through the square root of the Jensen–Shannon divergence,<sup>14</sup>

$$\sqrt{JS} = \sqrt{\frac{1}{2}\delta(p(\pi), m(\pi)) + \frac{1}{2}\delta(p'(\pi), m(\pi))}, \quad (2)$$

with  $m(\pi) = \frac{1}{2}(p(\pi) + p'(\pi))$  and  $\delta(P, Q) = \sum_i P \log\left(\frac{P}{Q}\right)$  being the Kullback–Leibler divergence for the discrete probability distributions  $P$  and  $Q$ . Note that, by construction,  $0 \leq \sqrt{JS} \leq 1$ .<sup>22</sup>

The HTa plane is, thus, constructed to easily compare  $\sqrt{JS}$  vs  $H[p]$ , with both metrics being defined in  $[0, 1]$ . This is the rationale behind a definition of the time asymmetry different from other proposals, as, e.g., Refs. 13 and 14, where Z-scores and p-values would not easily be comparable. The larger the  $\sqrt{JS}$ , the greater the level of temporal asymmetry; similarly, the higher the rate of  $H[p]$ , the more disordered the system dynamics is.

### C. Synthetic time series

In order to test the proposed HTa plane, we here first resort to synthetic time series obtained by the following well-known dynamical models:

**GLP** A Gaussian linear process  $x_t \sim \mathcal{N}(\mu, \sigma^2)$ ,  $\mu = 0$ ,  $\sigma = 1$ .

**AR(2)** A linear auto-regressive model of second order driven by a white noise  $\varepsilon_t$ , given by

$$x_{t+2} = 0.7x_{t+1} + 0.2x_t + \varepsilon_t.$$

**STAR(1)** A static nonlinear transition of a Gaussian process of first order, given by

$$x_t = \tanh^2(y_t), \text{ with } y_t = 0.6y_{t-1} + \varepsilon_t.$$

**NAR** Laplacian and bimodal. Two coupled nonlinear auto-regressive systems:

$$\begin{aligned} x_t &= 0.5x_{t-1} - 0.3x_{t-2} + 0.1y_{t-2} + 0.1x_{t-2}^2 \\ &\quad + 0.4y_{t-1}^2 + 0.0025\eta', \\ y_t &= \sin(4\pi t) + \sin(6\pi t) + 0.0025\eta''. \end{aligned}$$

Noises  $\{\eta', \eta''\}$  are, respectively, i.i.d. drawn from a Laplacian,

$$p(\eta) = \frac{1}{4b} \exp\left(\frac{-|\eta - \mu|}{b}\right), \mu = 0, b = 1,$$

and a bimodal distribution,

$$\begin{aligned} p(\eta) &= 0.5\mathcal{N}(\eta|\mu, \sigma) + 0.5\mathcal{N}(\eta|-\mu, \sigma). \\ \mu &= 0.63, \sigma = 1. \end{aligned}$$

**SETAR(2; 2,2)** Two switched nonlinear systems of self-exciting threshold AR (SETAR) type, characterized by

jumps between different nonlinear regimes with different delays.<sup>23,24</sup> This first one is a two regime model, each one with second-order delays,

$$x_t = \begin{cases} 0.62 + 1.25x_{t-1} - 0.43x_{t-2} + 0.0381\varepsilon_t & \text{if } x_{t-2} \leq 3.25 \\ 2.25 + 1.52x_{t-1} - 1.24x_{t-2} + 0.0626\varepsilon_t & \text{otherwise.} \end{cases}$$

**SETAR(2; 3,2)** A second model with two regimens with delays of third and second-orders,

$$x_t = \begin{cases} 0.733 + 1.047x_{t-1} - 0.007x_{t-2} + 0.242x_{t-3} \\ \quad + 0.0357\varepsilon_t & \text{if } x_{t-2} \leq 3.083 \\ 1.983 + 1.52x_{t-1} - 1.162x_{t-2} + 0.0586\varepsilon_t & \text{otherwise.} \end{cases}$$

**Rössler** The  $y$  variable in the chaotic regimen of the Rössler system, whose dynamics is given by

$$\begin{aligned} \dot{x} &= -y - z, \\ \dot{y} &= x + 0.2y, \\ \dot{z} &= 0.2 + z(x - 5.7). \end{aligned}$$

The generated time series have a length of  $M = 10^4$ , with an integration step of 0.01, after the first 1000 samples are removed to avoid potential transients.

**Lorenz** The  $z$  variable of the Lorenz dynamical system in its chaotic regime, defined as

$$\begin{aligned} \dot{x} &= 10(y - x), \\ \dot{y} &= x(28 - z) - y, \\ \dot{z} &= xy - 2.6667z. \end{aligned}$$

The time series length and integration step are the same as for the Rössler case.

### III. ANALYSIS OF SYNTHETIC TIME SERIES

We start analyzing synthetic time series created with the dynamical systems described in Sec. II C. Specifically, Fig. 1 reports the evolution of the position in the HTa plane of such time series by varying the embedding dimension  $D$  from 3 to 7. As is to be expected, reducing  $D$  moves all points toward the upper left corner (i.e.,  $H \rightarrow 1$  and  $\sqrt{JS} \rightarrow 0$ ), as the reduced resolution implies a loss of details about the dynamics and, hence, time series resembling more random ones. It is nevertheless interesting to note that the two metrics are partly independent and convey different information when different dynamical systems are compared. To illustrate, for a given value of  $D$ , the Rossler's  $Y$  and Lorenz'  $Z$  time series have very similar entropy  $H$ , but significantly different  $\sqrt{JS}$ . This is a first confirmation that the two metrics, in spite of being calculated over similar probability distributions, are able to independently represent the two target properties of the underlying dynamical system—i.e., entropy and time asymmetry.

We further move to the analysis of another classical aspect of time series, i.e., the presence of observational noise. Fig. 2, left panel,

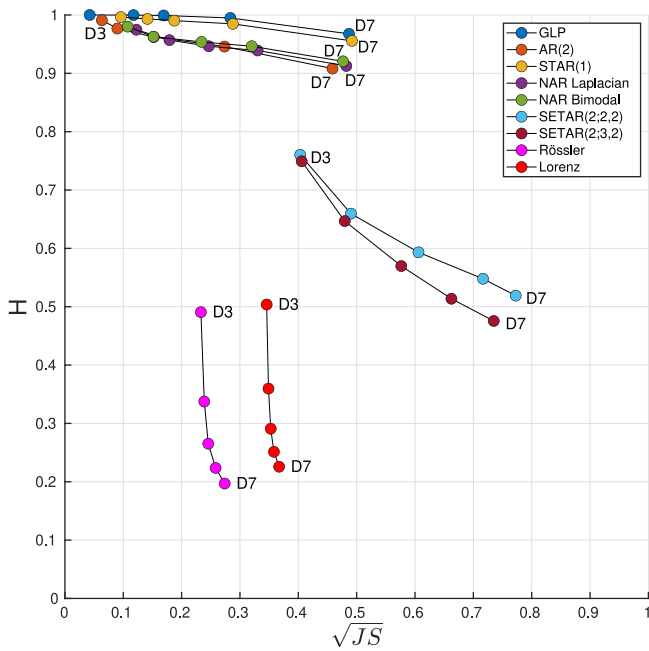


**FIG. 1.** Evolution on the  $H$ - $\sqrt{JS}$  plane of time series created with the dynamical systems listed in Sec. II C for different embedding dimensions  $D \in [3, \dots, 7]$ .

reports the evolution in the plane of time series  $x'_t = x_t + \varepsilon(\sigma')$  created with the same dynamical system  $x_t$ , for a fixed  $D = 5$ , with an increasing amount of observational noise  $\varepsilon(\sigma') \propto \mathcal{N}(0, \sigma'^2) | \sigma' = n\sigma_{x_t}$ , with  $0 \leq n \leq 3$ , and  $n \in \mathbb{R}$ . As is to be expected, also in this case, the two metrics tend to  $H \rightarrow 1$  and  $\sqrt{JS} \rightarrow 0$ ; i.e., the time series are becoming indistinguishable from a random noise—note that such values are never achieved due to finite size effects ( $M = 10^4$ ). To better visualize how sensitive the models are when changing the noise level, we compute the percentage of variation for  $\Delta H\% = 100 \cdot (H - H')/H$  and  $\Delta \sqrt{JS}\% = 100 \cdot (\sqrt{JS} - \sqrt{JS}')/\sqrt{JS}$ , with  $(*)'$  computed on  $x'$ . The right panels of Fig. 2 depict how the entropies for Lorenz and Rössler are modified even when the noise amplitude  $n$  is low, while the same does not happen for the time asymmetry.

Due to the above-mentioned difference, an interesting crossover appears such that, for instance, the Lorenz'  $Z$  time series strongly increases its entropy before the time asymmetry is affected. It, thus, crosses the SETAR's trajectory in the plane, for which the two metrics change with the same pace. In other words, this implies that, in general, given two time series with similar  $H$ s and  $\sqrt{JS}$ s, the addition of the same amount of observational noise may result in different values of these two metrics.

In order to better understand such a crossover, we first created  $10^4$  time series composed of 200 values in the range  $[0, 1]$ , with  $H = 0.6$  and  $\sqrt{JS} = 0.4$  ( $D$  is here fixed to 3). This has been achieved by starting with random time series, for then applying dual annealing optimization,<sup>25</sup> with the distance to these two values as the objective function to be minimized. Afterward, a small random

noise [drawn from  $\mathcal{N}(0, 0.02)$ ] is added to each time series, and the resulting  $H$  and  $\sqrt{JS}$  have been calculated. Panel (a) of Fig. 3 reports the final distribution of the values (gray squares, with darker colors indicating higher densities)—for reference, the starting point is marked with a red cross; see the bottom part of the plot. It can be appreciated that the noise always increases the entropy, as it may be expected; at the same time, it can both increase and decrease the time asymmetry, with values spanning from less than 0.3 to almost 0.5. Panel (b) of the same figure further reports the probability of finding a pattern with a turning point (i.e., a pattern in which the derivative changes sign or for which the intermediate point is a local minimum or maximum, e.g.,  $\pi = \{132\}$ ) in these time series as a function of the final  $\sqrt{JS}$ . Time series with a lower time asymmetry after the addition of noise are characterized by a small turning point probability and, thus, by a large number of continuously ascending and descending patterns (i.e., 123 and 321). It can, thus, be concluded that the presence of patterns with turning points is affecting the way the time asymmetry of the time series is modified by noise.

In order to confirm this, we have considered a minimal synthetic model, in which short time series  $(x_1, x_2, x_3, x_4)$  are created by drawing random numbers from a uniform distribution  $\mathcal{U}(0, 1)$  and are further normalized in the interval  $[0, 1]$ . We then add a small observational noise drawn from a normal distribution to these time series, obtaining a new set of time series  $(x'_1, x'_2, x'_3, x'_4)$ . Considering the original time series, the three initial values  $(x_1, x_2, x_3)$  must correspond to an ordinal pattern either with or without a turning point, i.e., either  $\pi_{1,\dots,4}$ , or  $\pi_{0.5}$ . Regarding the next pattern in the sequence, i.e., the one for  $(x_2, x_3, x_4)$ , it is worth noting that it is constrained by the previous one; specifically, after a pattern without a turning point, the probability of finding the same pattern is approximately 25% [see the dashed gray line in panel (c) of Fig. 3]; on the other hand, a given pattern with a turning point can never be followed by the same one by construction. We then calculated the probability of finding the same pattern in  $(x'_1, x'_2, x'_3)$  and  $(x'_2, x'_3, x'_4)$  as a function of the standard deviation of the added noise for original time series with [blue line in panel (c) of Fig. 3] and without (magenta line in the same panel) turning points.

An interesting conclusion can be drawn. When the original time series starts with an ordinal pattern without turning points, the probability of ending up with a time series with two identical ordinal patterns is lower than the initial probability of finding such pattern combination. On the other hand, the former probability is always higher than the latter in the case of an initial ordinal pattern with turning points simply because the latter is zero; i.e., a turning point pattern cannot be repeated twice. In other words, the addition of noise has a completely different effect in these two cases: it can both reduce and increase the probability of finding the same pattern twice. If the original time series has a large share of turning point patterns, the result can be the appearance of many pairs of identical patterns, which in turn have the effect of increasing  $\sqrt{JS}$ . Note that this does not necessarily disagree with previous theoretical results,<sup>26</sup> as such behavior is caused by the way time asymmetry is measured and the limited size of the time series.

It is interesting to note that the appearance of both turning points and repeated ordinal patterns is a function of the autocorrelation of the time series; as such, it may be speculated that this latter aspect may be responsible for the different evolution of the

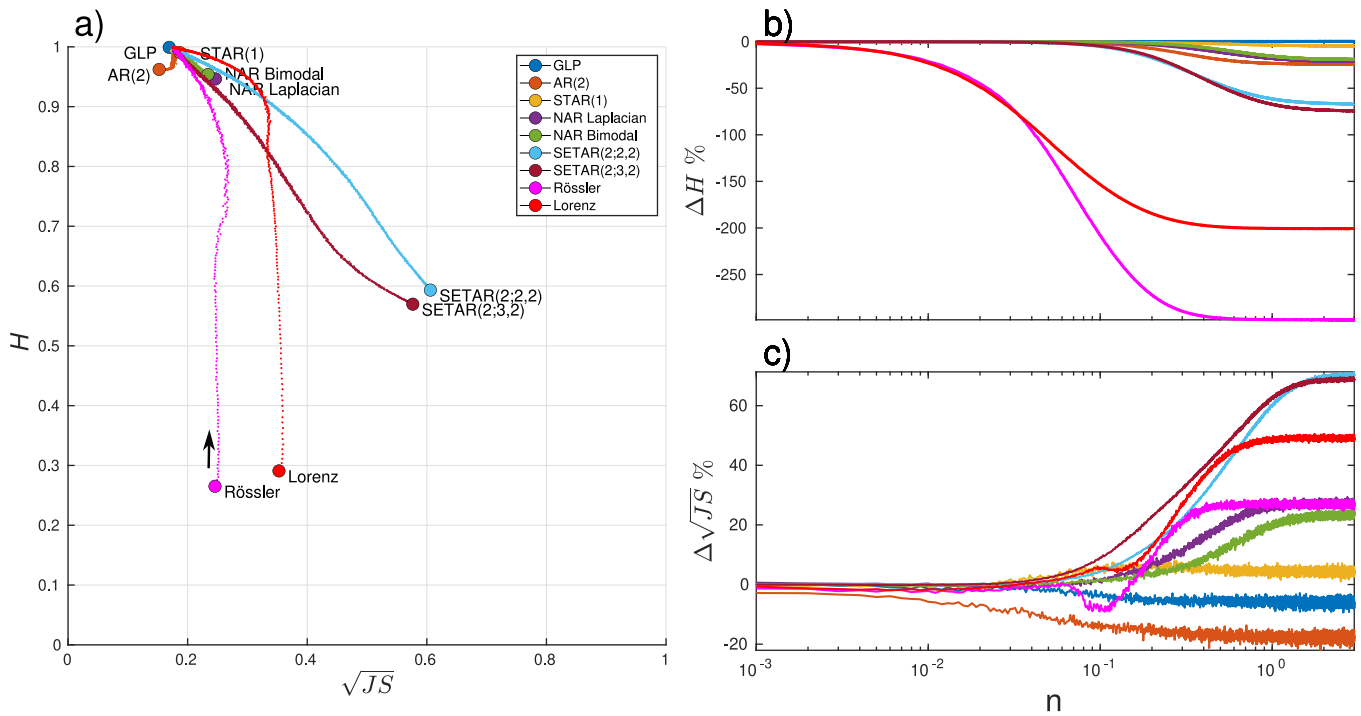


**FIG. 2.** Left panel: Evolution on the  $H$ - $\sqrt{JS}$  plane of time series created with the dynamical systems listed in Sec. II C, for  $D = 5$ , and different levels of observational noise  $\varepsilon(\sigma')$ . Each point corresponds to the average of 50 independent realizations. The direction of increasing levels of noise is represented by the black arrow. Right panels: Evolution of the percentage of variation of  $H$  [panel (b)] and  $\sqrt{JS}$  [panel (c)] as a function of the noise amplitude  $n$ .

time asymmetry in the presence of noise. In order to test this, we have considered the  $10^4$  synthetic time series previously presented and calculated the correlation coefficient between their autocorrelation using a lag of 1 on one hand and the difference between the  $\sqrt{JS}$  before and after the addition of the noise on the other hand. The result ( $\rho = -0.65, p\text{-value} < 0.01$ ) indicates that both properties are indeed connected, with  $\sqrt{JS}$  decreasing in highly autocorrelated time series—even if true causality cannot be guaranteed at this stage.

This is not the first time that the importance of such points in the calculation of the permutation entropy has been highlighted, see, for instance, Refs. 27–29. While they seem to have a major impact in the time asymmetry of noisy time series, turning points have only been studied for  $D = 3$ .<sup>28,29</sup> Their presence cannot be defined for higher embedding dimensions, as an ordinal pattern of order  $D$  can contain up to  $D - 2$  peaks—in other words, multiple local turning points can coexist in a large pattern, thus suggesting that a more appropriate concept would be the one of “turning point density.” Still, multiple relationships between such density, observational noise, and the time series’ irreversibility and autocorrelation structures may constitute an interesting open problem.

#### IV. ANALYSIS OF REAL-WORLD DATA

In order to provide an overview of the type of results that may be obtained using the proposed HTa plane, we here analyze

three sets of data, respectively, representing biological, financial, and technological real-world systems.

##### A. Brain dynamics in schizophrenia

Starting from a biological system, we characterize time series of electroencephalography (EEG) data corresponding to control (healthy) subjects and patients suffering from schizophrenia. Two independent data sets have here been considered. The first one (denoted as EEG I), freely available at <https://doi.org/10.18150/repod.0107441>, includes data recorded in an eyes-closed resting state condition, with a 250 Hz sampling frequency, for a length of approximately 15 min—or approximately 220 000 samples per time series.<sup>30</sup> The second one (EEG II), made available by the Laboratory for Neurophysiology and Neuro-Computer Interfaces of the M. V. Lomonosov Moscow State University at [http://brain.bio.msu.ru/eeg\\_schizophrenia.htm](http://brain.bio.msu.ru/eeg_schizophrenia.htm), has a sampling frequency of 128 Hz, and the time series have a length of 1 min—note that no additional information on the recording procedure seems to be available. For the sake of clarity, results here reported only correspond to the O2 sensor, whose dynamics was previously found to be altered in this pathology.<sup>30–32</sup>

The results of the analysis of the raw time series of both data sets are depicted in panels (a) and (c) of Fig. 4. Two interesting facts can be appreciated. First of all, there is a large difference in the

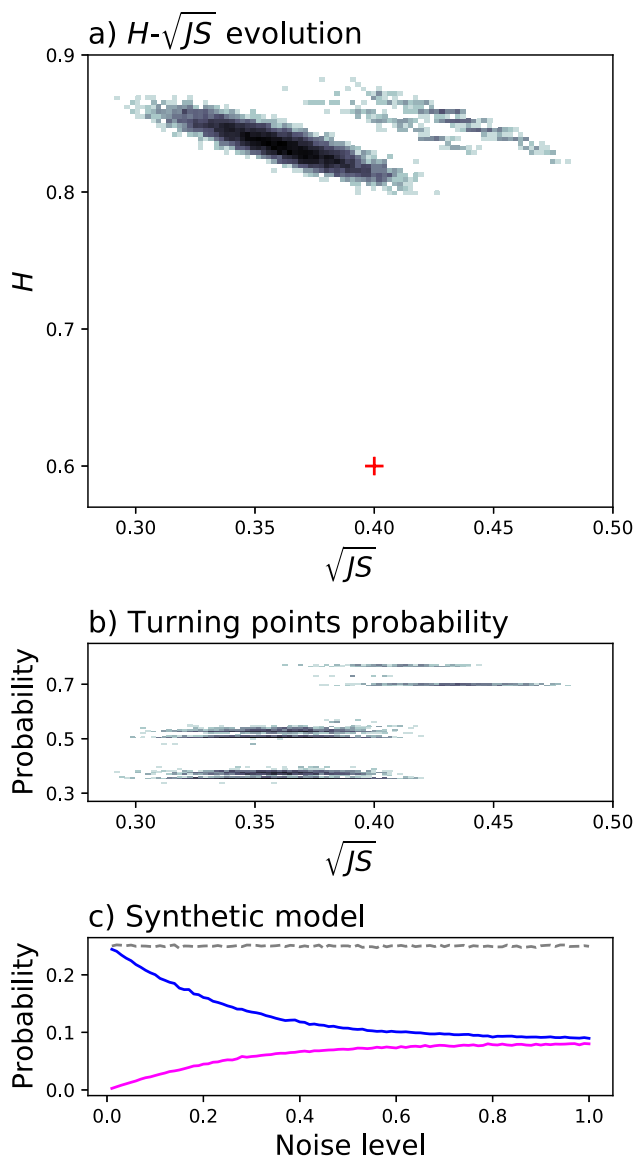


**FIG. 3.** Evolution of  $H$  and  $\sqrt{JS}$  with observational noise. (a) Evolution in the entropy–asymmetry plane of  $10^4$  time series with  $H = 0.6$  and  $\sqrt{JS} = 0.4$  (red cross) after applying a small amount of noise (gray scale). (b) Probability of finding a turning point in the previous time series, before the noise is added, as a function of the final  $\sqrt{JS}$ . (c) Probability of finding two identical consecutive permutation patterns in a synthetic model when the original time series starts with an ordinal pattern with (magenta line) and without (blue line) a turning point as a function of the amplitude of the added observational noise.  $D = 3$  in all cases. See the main text for details on time series generation and on the synthetic model.

average  $H$  of both groups in the case of EEG I (0.853 for control subjects and 0.755 for patients), which is nevertheless lost in the case of EEG II. Note that for the sake of facilitating comparisons, panels (a)–(c) have the same axes’ limits. In order to check whether this

is caused by the different frequency resolution, we downsampled the time series of EEG I to match the frequency of EEG II using a Fourier method. Results, reported in panel (b), suggest that the differences in  $H$  between both groups are indeed located in higher frequencies, not available in the case of EEG II.

As a second point, the two data sets seem to yield heterogeneous results even when the sampling frequency is made equal. Specifically, by comparing panels (b) and (c), it can be appreciated that the  $\sqrt{JS}$  is slightly larger for control subjects in the case of EEG I, while the opposite is true for EEG II. It is difficult to pinpoint the reasons behind those discrepancies, as they may be the results of differences in the acquisition protocols, in data pre-processing, or even in patients’ inclusion and exclusion criteria. To illustrate, it has previously been shown that an eyes-open resting state is characterized by higher time irreversibility than an eyes-closed one.<sup>33</sup> Additionally, schizophrenia is a complex condition with many phenotypes and potentially many etiologies, which may impact the way brain time irreversibility is observed.<sup>34</sup> In short, the first three panels of Fig. 4 highlight both the sensitivity of this plane representation and the importance of providing precise methodological information when sharing data sets, especially biomedical ones.

## B. Cryptocurrencies and financial markets

We then move to the analysis of financial systems, starting with three cryptocurrencies and the evolution of their value through time: Bitcoin, Ethereum, and Litecoin. These three have been chosen for representing different stages in the life of these financial instruments, corresponding to the 1st, 2nd, and 20th cryptocurrencies by market capitalization and, therefore, represent both mature and niche assets. Time series correspond to the evolution of prices against the US dollar with a 1-min resolution, freely available at <https://www.cryptodatadownload.com/data/gemini/>. These time series correspond to years 2015–2020 for Bitcoin, 2016–2020 for Ethereum, and 2018–2020 for Litecoin.

Results for these three cryptocurrencies and by year are reported in panel (d) of Fig. 4, with the symbol shape representing the asset and colors the considered year. The heterogeneity of these assets is evident, with values covering the whole plane. It is especially noteworthy the case of Bitcoin, which has moved from extremely high time asymmetry for year 2015 to a highly random dynamics in 2020. The position in the plane is able to describe how the efficiency (according to the efficient market hypothesis<sup>35,36</sup>) of this asset has increased with time, in parallel with the increase in its market capitalization. The plane also highlights the inefficient dynamics of Litecoin, which still has high time asymmetry and low entropy after three years of trading.

Panel (e) of Fig. 4 additionally reports the evolution of the two considered metrics for time series of three well-known US market indices: the Dow Jones Industrial Average (DJIA), the NASDAQ Composite Index (NASDAQ), and the Standard and Poor’s 500 index (SP500). Data, freely available at <https://firstratedata.com>, correspond to the time period 1–14 April 2022 and are sampled with 1, 5, 30, and 60 min time resolutions. It can be observed that the values yielded by the three indices are comparable at high time resolutions and that they appear to be more random for 1 and 5 min resolutions when compared to the 60 min case.

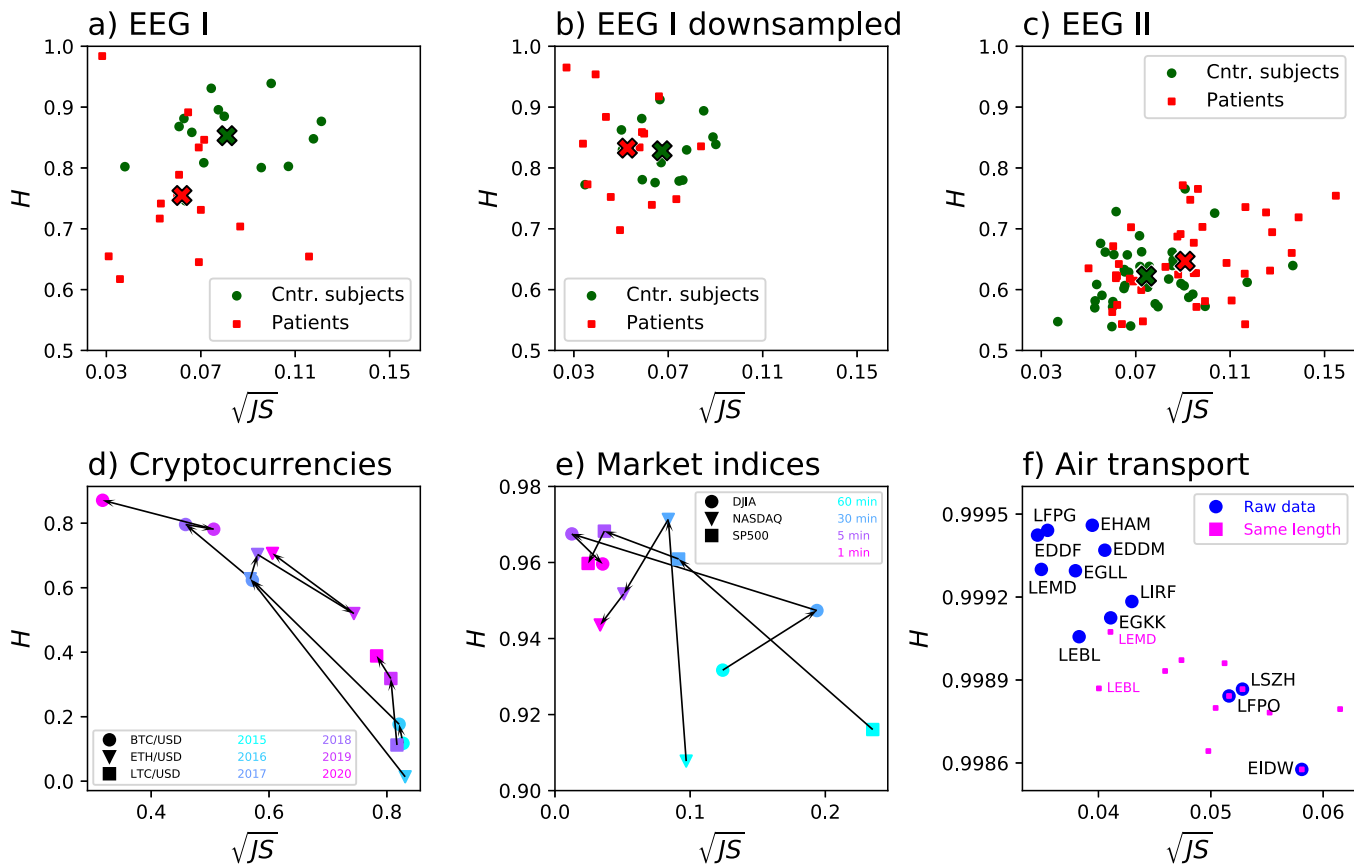


**FIG. 4.** Entropy–asymmetry plane for several real-world systems. Panels (a) and (c) reports the results for two EEG data sets, with panel (b) corresponding to the first data set with time series being downsampled to have the same resolution as the second one. Green circles and red squares, respectively, correspond to control subjects and patients and crosses to the median of each group. Note that axes’ limits are the same in all panels to facilitate comparisons. Panel (d): evolution of three cryptocurrencies through time. Panel (e): Evolution of three US stock market indices as a function of the time resolution of the data. Panel (f): results for time series representing delays at landing at 12 major European airports; blue circles correspond to the complete time series and purple squares to the time series trimmed in order to have the same length.

### C. Delays in air transport

We finally analyze an example of a technological system and specifically the evolution of delays in air transport. We extracted time series of delays at landing for aircraft arriving at the 12 largest European airports. Data have been obtained from the EUROCONTROL’s R&D Data Archive, freely accessible at <https://www.eurocontrol.int/dashboard/rnd-data-archive>, and correspond to all operations executed throughout September 2018. The landing delay of each flight arriving at those 12 airports has been estimated as the difference between the actual and planned landing times. These values have then been concatenated according to the arrival sequence, in order to create a single time series per airport, in which each element is the delay of a single aircraft.

The results for the raw time series are reported in panel (f) of Fig. 4, blue circles. Two general trends can be observed: first, all time series have large values of  $H$  and low values of  $\sqrt{JS}$ , suggesting highly random dynamics; and second, smaller airports (as, e.g., EIDW—Dublin Airport, LFPO—Paris Orly Airport, or

LSZH—Zurich Airport) are less random than larger ones. It has nevertheless to be noted that these differences may be due to the different length of each time series—larger airports operate more aircraft, and hence, their time series contain more values. In order to solve this, purple points in the same panel report the values of the metrics when the same quantity of data is used for each airport—i.e., longer time series are trimmed to match the length of the shortest one. A similar trend is still observed, albeit with differences between large and small airports being less marked.

In a way similar to the efficient market hypothesis, one may expect the delay of consecutive landing flights to be independent if the airport is efficient. In other words, if an airport is efficient in the sense of being able to accommodate aircraft as soon as they arrive, delays should be random events, independent from each other, and only due to exogenous factors. On the other hand, any departure from complete randomness implies that delays are not independent, that they propagate between consecutive landing operations, and, thus, that are the result of inefficiencies at the arrival airport—e.g.,

lack of landing capacity. The minor temporal asymmetry seen in Fig. 4 suggests that some correlations are present between delays of consecutive landing events, especially for smaller airports, in turn pointing toward a lack of resources (specifically, landing capacity) or flexibility as a potential cause.

## V. DISCUSSION AND CONCLUSIONS

In this contribution, we have analyzed the relationship between two metrics that can be extracted from time series using the well-known paradigm of ordinal patterns, i.e., the permutation entropy  $H$  and the time asymmetry  $\sqrt{S}$ . The underlying physical concepts are not independent, with the latter being defined as the rate of production of the former; and, more importantly, both are here calculated from different aggregations of the same ordinal pattern probabilities  $p(\pi)$ . One may, thus, expect these two metrics to be highly correlated and eventually redundant.

By reconstructing an entropy–time asymmetry (HTa) plane, we have shown that this is indeed not the case. Specifically, time series generated by different dynamical systems may have similar values in one of the metrics, yet being substantially different according to the other one—see, for instance, the case of Rossler’s  $Y$  and Lorenz’  $Z$  time series in Fig. 1. We have also shown that the time asymmetry is highly sensitive to the presence of ordinal patterns with turning points. Consequently, this metric can evolve differently when observational noise is added, leading to the appearance of crossovers between different dynamical systems—see Fig. 2. Yet, turning points are ill-defined for  $D > 3$ : a generalization of the observed phenomenon to higher pattern dimensions may constitute an interesting open topic. Note that a consistent increase in the time asymmetry as a result of the presence of observational noise is theoretically impossible<sup>26</sup> and may, therefore, be attributed to the use of ordinal patterns; see also Ref. 11 for a discussion.

Additionally, the analyses based on real-world data presented in Sec. IV highlight two interesting facts. First of all, the entropy and time asymmetry can be correlated, as shown in the case of cryptocurrencies and air transport; and a higher entropy usually implies a smaller time asymmetry. This is to be expected, especially for large values of  $H$ , as some degree of heterogeneity between ordinal pattern probabilities is required to have a time asymmetry; the latter necessarily has to tend to 0 when  $H \rightarrow 1$ . At the same time, both metrics can also evolve in an independent way, thus highlighting different aspects of the time series under analysis—the clearest example can be seen in the case of the EEG data sets. Second, the plane is highly sensitive to the characteristics of the time series. As seen in Fig. 4, the presence of pathology can affect these metrics in opposite directions, even when the EEG time series correspond to the same sensor, depending on how they have been recorded and pre-processed. Such sensitivity is a positive aspect, in that it allows describing even small differences in the data, but, at the same time, highlights the importance of relying on homogeneous and well-described data.

## ACKNOWLEDGMENTS

This project has received funding from the European Research Council (ERC) under the European Union’s Horizon 2020 research and innovation program (Grant Agreement No. 851255). J.H.M.

acknowledges funding from the project PID2020-113737GB-I00 of MCIN/AEI/10.13039/501100011033. J.J.R. acknowledges support from MCIN/AEI/10.13039/501100011033/FEDER/EU under project APASOS (PID2021-122256NB-C22). This work has been partially supported by the Mariía de Maeztu project CEX2021-001164-M funded by the MCIN/AEI/10.13039/501100011033.

The authors would like to thank M. Chavez and E. Martínez for valuable conversations.

## AUTHOR DECLARATIONS

### Conflict of Interest

The authors have no conflicts to disclose.

### Author Contributions

**Johann H. Martínez:** Conceptualization (equal); Methodology (equal); Writing – original draft (equal). **José J. Ramasco:** Conceptualization (equal); Methodology (equal); Writing – original draft (equal). **Massimiliano Zanin:** Conceptualization (equal); Methodology (equal); Writing – original draft (equal).

## DATA AVAILABILITY

The data that support the findings of this study are openly available in RepOD at <https://doi.org/10.18150/repod.0107441> (first schizophrenia EEG data set), [http://brain.bio.msu.ru/eeg\\_schizophrenia.htm](http://brain.bio.msu.ru/eeg_schizophrenia.htm) (second schizophrenia EEG data set), <https://www.cryptodatadownload.com/data/gemini/> (cryptocurrency data set), <https://firstratedata.com> (market indices), and <https://www.eurocontrol.int/dashboard/rnd-data-archive> (air transport data set). In the case of air transport, derived (pre-processed) data are available from the corresponding author upon reasonable request.

## REFERENCES

- D. M. Dinitto, R. R. Mcdaniel, Jr., T. W. Ruefli, and J. B. Thomas, “The use of ordinal time-series analysis in assessing policy inputs and impacts,” *J. Appl. Behav. Sci.* **22**, 77–93 (1986).
- C. Bandt and B. Pompe, “Permutation entropy: A natural complexity measure for time series,” *Phys. Rev. Lett.* **88**, 174102 (2002).
- M. Zanin and F. Olivares, “Ordinal patterns-based methodologies for distinguishing chaos from noise in discrete time series,” *Commun. Phys.* **4**, 190 (2021).
- J. Amigó, *Permutation Complexity in Dynamical Systems: Ordinal Patterns, Permutation Entropy and All That* (Springer Science & Business Media, 2010).
- M. Zanin, L. Zunino, O. A. Rosso, and D. Papo, “Permutation entropy and its main biomedical and econophysics applications: A review,” *Entropy* **14**, 1553–1577 (2012).
- M. Riedl, A. Müller, and N. Wessel, “Practical considerations of permutation entropy,” *Eur. Phys. J.: Spec. Top.* **222**, 249–262 (2013).
- K. Keller, T. Mangold, I. Stolz, and J. Werner, “Permutation entropy: New ideas and challenges,” *Entropy* **19**, 134 (2017).
- I. Leyva, J. H. Martínez, C. Masoller, O. A. Rosso, and M. Zanin, “20 years of ordinal patterns: Perspectives and challenges,” *Europhys. Lett.* **138**, 31001 (2022).
- É. Roldán and J. M. Parrondo, “Estimating dissipation from single stationary trajectories,” *Phys. Rev. Lett.* **105**, (9) 150607 (2010).
- A. Puglisi and D. Villamaina, “Irreversible effects of memory,” *Europhys. Lett.* **88**, 30004 (2009).
- M. Zanin and D. Papo, “Algorithmic approaches for assessing irreversibility in time series: Review and comparison,” *Entropy* **23**, 1474 (2021).

- <sup>12</sup>G. Graff, B. Graff, A. Kaczowska, D. Makowiec, J. Amigó, J. Piskorski, K. Narkiewicz, and P. Guzik, "Ordinal pattern statistics for the assessment of heart rate variability," *Eur. Phys. J.: Spec. Top.* **222**, 525–534 (2013).
- <sup>13</sup>M. Zanin, A. Rodríguez-González, E. Menasalvas Ruiz, and D. Papo, "Assessing time series reversibility through permutation patterns," *Entropy* **20**, 665 (2018).
- <sup>14</sup>J. H. Martínez, J. L. Herrera-Diestra, and M. Chavez, "Detection of time reversibility in time series by ordinal patterns analysis," *Chaos* **28**, (14) 123111 (2018).
- <sup>15</sup>J. Li, P. Shang, and X. Zhang, "Time series irreversibility analysis using Jensen–Shannon divergence calculated by permutation pattern," *Nonlinear Dyn.* **96**, 2637–2652 (2019).
- <sup>16</sup>W. Yao, W. Yao, J. Wang, and J. Dai, "Quantifying time irreversibility using probabilistic differences between symmetric permutations," *Phys. Lett. A* **383**, 738–743 (2019).
- <sup>17</sup>M. Martin, A. Plastino, and O. Rosso, "Generalized statistical complexity measures: Geometrical and analytical properties," *Phys. A* **369**, 439–462 (2006).
- <sup>18</sup>J. M. Amigó, S. Zambrano, and M. A. Sanjuán, "True and false forbidden patterns in deterministic and random dynamics," *Europhys. Lett.* **79**, (18) 50001 (2007).
- <sup>19</sup>A. Popov, O. Avilov, and O. Kanaykin, "Permutation entropy of EEG signals for different sampling rate and time lag combinations," in *2013 Signal Processing Symposium (SPS)* (IEEE, 2013), pp. 1–4.
- <sup>20</sup>F. Olivares and L. Zunino, "Multiscale dynamics under the lens of permutation entropy," *Phys. A* **559**, 125081 (2020).
- <sup>21</sup>M. Chavez and J. H. Martínez, "Ordinal spectrum: A frequency domain characterization of complex time series," [arXiv:2009.02547](https://arxiv.org/abs/2009.02547) (2020).
- <sup>22</sup>J. Lin, "Divergence measures based on the Shannon entropy," *IEEE Trans. Inf. Theory* **37**, 145–151 (1991).
- <sup>23</sup>H. Tong, *Threshold Models in Non-Linear Time Series Analysis* (Springer Science & Business Media, 2012), Vol. 21.
- <sup>24</sup>H. Tong, "Threshold models in time series analysis—30 years on," *Stat. Interface* **4**, 107–118 (2011).
- <sup>25</sup>Y. Xiang and X. Gong, "Efficiency of generalized simulated annealing," *Phys. Rev. E* **62**, 4473 (2000).
- <sup>26</sup>A. Porporato, J. R. Rigby, and E. Daly, "Irreversibility and fluctuation theorem in stationary time series," *Phys. Rev. Lett.* **98**, 094101 (2007).
- <sup>27</sup>L. Zunino, F. Olivares, A. F. Bariviera, and O. A. Rosso, "A simple and fast representation space for classifying complex time series," *Phys. Lett. A* **381**, 1021–1028 (2017).
- <sup>28</sup>S. Berger, G. Schneider, E. F. Kochs, and D. Jordan, "Permutation entropy: Too complex a measure for EEG time series?," *Entropy* **19**, 692 (2017).
- <sup>29</sup>C. Bandt, "Order patterns, their variation and change points in financial time series and Brownian motion," *Stat. Pap.* **61**, 1565–1588 (2020).
- <sup>30</sup>E. Olejarczyk and W. Jernajczyk, "Graph-based analysis of brain connectivity in schizophrenia," *PLoS One* **12**, e0188629 (2017).
- <sup>31</sup>M. Sabeti, S. Katebi, and R. Boostani, "Entropy and complexity measures for EEG signal classification of schizophrenic and control participants," *Artif. Intell. Med.* **47**, 263–274 (2009).
- <sup>32</sup>B. Raghavendra, D. N. Dutt, H. N. Halahalli, and J. P. John, "Complexity analysis of EEG in patients with schizophrenia using fractal dimension," *Physiol. Meas.* **30**, 795 (2009).
- <sup>33</sup>M. Zanin, B. Güntekin, T. Aktürk, L. Hanoğlu, and D. Papo, "Time irreversibility of resting-state activity in the healthy brain and pathology," *Front. Physiol.* **10**, 1619 (2020).
- <sup>34</sup>K. R. Patel, J. Cherian, K. Gohil, and D. Atkinson, "Schizophrenia: Overview and treatment options," *Pharm. Ther.* **39**, 638 (2014).
- <sup>35</sup>E. F. Fama, "Efficient capital markets: A review of theory and empirical work," *J. Finance* **25**, 383–417 (1970).
- <sup>36</sup>E. F. Fama, "Market efficiency, long-term returns, and behavioral finance," *J. Financ. Econ.* **49**, 283–306 (1998).